Light-Induced Unlocking Reactivity of Fragments for Fast Target-Guided Synthesis of Carbonic Anhydrase Inhibitors

Chloé Puteaux, Isabelle Toubia, Lina Truong, Marie Hubert-Roux, Laetitia Bailly, Hassan Oulyadi, Pierre-yves Renard, Cyrille Sabot

Light-Induced Unlocking Reactivity of Fragments for Fast Target-Guided Synthesis of Carbonic Anhydrase Inhibitors

Chloé Puteaux, Isabelle Toubia, Lina Truong, Marie Hubert-Roux, Laetitia Bailly, Hassan Oulyadi, Pierre-Yves Renard, and Cyrille Sabot*

* Dr. C. Puteaux, Dr. I. Toubia, L. Truong, Dr. M. Hubert, L. Bailly, Prof. Dr. H. Oulyadi, Prof. Dr. P.-Y. Renard, Dr. C. Sabot
Normandie, Univ Rouen Normandie, INSA Rouen, CNRS, Normandie Univ, COBRA UMR 6014, INC3MFR 3038, F-76000 Rouen, France
E-mail: cyrille.sabot@univ-rouen.fr

Abstract: We showcase the successful combination of photochemistry and kinetic target-guided synthesis (KTGS) for rapidly pinpointing enzyme inhibitors. KTGS is a fragment-based drug discovery (FBDD) methodology in which the biological target (BT) orchestrates the construction of its own ligand from fragments featuring complementary reactive functionalities. Notably, fragments interacting with the protein binding sites leverage their spatial proximity, facilitating a preferential reaction. Consequently, the resulting bivalent ligand exhibits heightened affinity. Within the realm of KTGS strategies, *in situ* click chemistry stands out as the most widely used to identify potent protein binders. This approach requires significant protein contributions, such as binding interactions and appropriate orientations of fragments, to overcome high activation barriers. This leads to prolonged incubation times and the potential for generating false negatives, thereby limiting this strategy to proteins that are stable enough in buffer. We herein unveil the possibility to integrate photochemistry into the realm of KTGS, accelerating the ligation reaction between fragments to a time scale of minutes. This approach should significantly expand the narrow reactivity window of traditional KTGS reactions, paving the way for the exploration and development of novel photo-KTGS reactions.

Introduction

Fragment-based drug discovery (FBDD) is a process that employs small molecular-weight molecules exhibiting low affinities but forming high-quality binding interactions with the protein of interest (POI). Such small molecules or fragments are usually pinpointed by robust biophysical screening techniques like nuclear magnetic resonance (NMR) spectroscopy, surface plasmon resonance (SPR) experiments, and X-ray crystallography, all of which possess the sensitivity to detect weak interactions.[1] FBDD generally requires much smaller collections of molecules as compared to conventional HTS (high-throughput screening), while giving rise to hits with high ligand-efficiency.

Biophysical assays have dramatically simplified the discovery of new fragments, yet the real challenge emerges in transforming or combining these fragments into potent hit compounds. The journey from fragments identification to their integration into a hit is critical, as these components must not only interact with distinct binding sites on the protein of interest but also preserve their original binding mode and dynamics when combined.[2], [3] Both the size and positioning of the chemical linker combining the fragments within the POI are important and should be taken into consideration. Kinetic target-guided synthesis (KTGS) is a strategy where the POI can select two binders from a library of fragments and induce their combination through irreversible bond formation in a single-step process.[4] This process aims to avoid the time-consuming steps of preparing (synthesis, purification, characterization) and testing all compounds in the library, particularly since many of them are inactive or lack the desired biological activity. KTGS will not succeed if the corresponding linker encounters steric clashes or unfavorable interactions, preventing its proper accommodation in the binding site.[5] The use of an anchor fragment is often a prerequisite to increase the chances of successful screening; however, a specific understanding of the second fragment binding mode is not necessary. *In situ* click chemistry, pioneered by Sharpless and colleagues,[6] is the most commonly used KTGS reaction for the identification of multisite ligands, accounting for more than 75% of KTGS experiments in 2020.[4a] The POI accelerates the linkage between two fragments bearing azide and alkyne chemical function, respectively, through a 1,3-dipolar cycloaddition forming a triazole linker. Azide and alkyne functions are small and readily incorporated into fragments or building-blocks. Furthermore, the formed triazole scaffold is able to add stabilizing interactions such as π-stacking, van der Waals, and hydrogen-bonding interactions with the POI.[7] Over the years, this strategy has shown to be very powerful for a large variety of proteins or nucleic acids and is a potent strategy for probing the chemical space surrounding the anchoring fragment.

However, one significant limitation is the omnipresent risk of generating false negatives—fragments that do not form a ligand *in situ* despite their affinity, and the affinity of the firmed ligand.[8] *In situ* click chemistry necessitates substantial protein contributions (entropic and enthalpic), to overcome high (3+2) cycloaddition reaction activation barriers (>25-30 kcal/mol).[5] This results in notably low reaction rates for forming the ligand. Prolonged incubation times are required in order to counterbalance this low reactivity (up to days or weeks), which can be detrimental for protein stability and, consequently, for the outcome of the KTGS. Through a recent retrospective analysis, we noticed that the reactions successfully employed in KTGS (thiol-alkylation,[9] thiol-Michael,[10] sulfo-click,[11]…) fall within a specific range of reactivity (reaction kinetics in the 10^{-6} to 10^{-1} M^{-1} s^{-1} range) (Figure 1).[12] Moreover, the use of faster reactions is not feasible, as the acceleration of product formation by the POI would no longer be noticeable, given the excessive product formation in the blank, or would require the implementation of competitive reactions more difficult to carry out.[9]

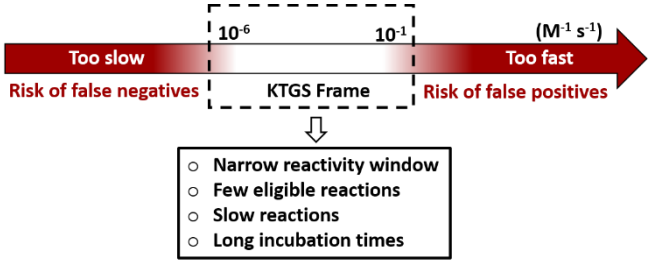

Figure 1. Chemical reactivity window of KTGS reactions.[12]

Facing this dilemma, we wondered if combining photochemical transformations with the KTGS strategy could constitute a solution to accelerate these reactions to an unprecedented level (Figure 2b). Photochemical reactions can provide highly reactive species with a spatial and temporal control upon external light stimulus. As a result, the ligation reaction could be triggered once the two building blocks rest in their respective protein binding site. On the other hand, reactive species resulting from unbound building blocks in aqueous solution, should rapidly react with nearby water molecules, thereby failing to promote ligand formation. In this way, we believed that both false positives and false negatives should be avoided or minimized, while maintaining fast kinetics.

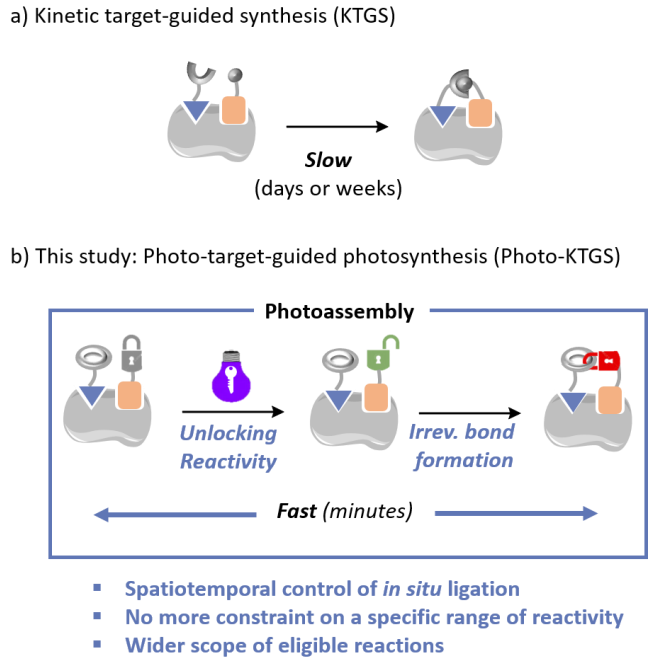

Figure 2. Traditional KTGS and current Photo-KTGS approach.

One key feature will be the selection of the photoinduced reaction that releases the reactive intermediate. If this intermediate is too reactive or lacks selectivity, it may also form a covalent bond with a fragment of the protein, as desired in photoaffinity labeling assays, leaving the second fragment untouched. Herein, we demonstrate that photoactivated 3-trifluoromethyl-3-phenyldiazirines (TPD) can be used as reactive partners in combination with thiols to recruit protein binders through fragments covalent attachment. The proof of concept is demonstrated with the metalloenzyme carbonic anhydrase. A systematic study was performed to examine potential benefits and limitations of this strategy.

Results and Discussion

Preliminary studies to examine the eligibility of TPD

TPD generate on-demand carbenes by losing a molecule of nitrogen upon light irradiation. Such high-energy intermediates are capable of reacting with heteronucleophiles X-H (X = N, S, O) but also unactivated C-H bonds, by inserting the formed carbene within the X-H bond.

We turned our attention towards the use of TPD as carbene precursors in the context of KTGS, for several reasons:

1) The photolysis is rapid and proceeds at ~350–360 nm, which is less damaging to proteins than other reactive moieties released at shorter wavelengths such as phenyl azides (250 nm irradiation is required to form the nitrene);

2) There is no intramolecular rearrangement of carbene intermediates, except for the formation of stable diazo isomers, which represent approximately 35% of the total yield.[13] Indeed, while aliphatic diazirines seem at first sight more appealing due to their smaller size, they undergo internal rearrangement through 1,2-hydrogen migration and yield the formation of diazo isomers to a large extent. This makes them prone to protonation and subsequent nucleophilic attack by carboxylic acids.[14] On the other hand, TPD generate inert diazo isomers, avoiding unwanted reactions outside the POI;[13]

3) Carbenes are also prone to rapid quenching by water molecules, with a lifespan in the nanosecond range in aqueous solution ($k = 3.1\ 10^8\ s^{-1}$).[15] It is an important feature for their use in KTGS, as non-specific ligation reactions between fragments occurring outside the protein-binding pocket should be minimized to facilitate the identification of protein-accelerated ligand formation;

4) The derivatization, handling and storage of TPD are facilitated by their exceptional stability under a variety of conditions such as acids, bases, laboratory ambient lights, and display thermal stability for at least 30 minutes at temperature as high as 75 °C;[13]

TPD introduced in the early 80's by Brunner *et al.* are widely used as photolabeling agents to trap non-covalent interactions with proteins through reactions between carbenes and adjacent amino acid residues in photoaffinity labelling experiments. Although lacking apparent chemoselectivity, we believed this might not necessarily be a hurdle to using TPD in a process under kinetic control. This paradigm shift was motivated by the fact that carbenes rapidly coordinate to the occupied p-orbitals of heteroatoms, leading to their rapid reaction with heteronucleophiles. In contrast, lifetime of carbenes in apolar solvents such as cyclohexane is much longer due to significantly lower C-H insertion reactivity.[13] Platz and Watt observed that sulfur-containing compounds such as thiols and disulfides were the most rapid to scavenge phenyl(trifluoromethyl)carbenes (PTC).[15] More recently, Kanoh *et al.* showed that amine and thiol functions tend to react with high selectivity with PTC.[16] Likewise,

Woo recently showed that cysteine was the most reactive amino acid towards TPD-based carbene under neat conditions.[17] However, no products with any amino acids were detected in aqueous conditions, presumably due to quenching of the carbene intermediate by water molecules. Higher concentrations of cysteine solutions were required to detect the adduct again. We also observed that thiol has proved to be an effective partner for KTGS (Figure 3). Individual and competitive reactions were conducted with two other main classes of heteronucleophiles: alcohols and amines, all three containing nonpolar C-H bonds. Reactions were carried out with diazirines **1a** and **1b** in the presence of an excess of heteronucleophiles (10 eq.) in acetonitrile, irradiated with a 365 nm-centered LED for 5 minutes. X-H insertion products were quantified by HPLC against an internal standard (Figure 3b).

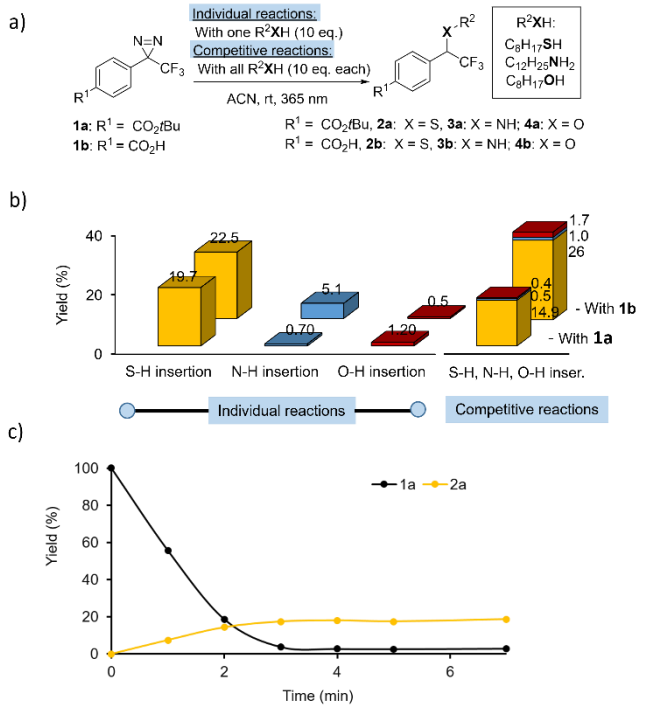

Figure 3. a) Individual or competitive photochemical reactions between diazirines **1a**-**b** (40 mM) and 1-octanethiol (400 mM, 10 eq), dodecylamine, (400 mM, 10 eq) and octan-1-ol (400 mM, 10 eq.) in ACN under a 365 nm-centered LED. b) Corresponding histograms obtained either from individual reactions (10 eq of thiol, amine or alcohol) or from competitive experiments (thiol, amine and alcohol, 10 eq. each), with yields quantified by HPLC against an internal standard. c) Time-dependent product **2a** formation and diazirine **1a** consumption for the reaction of **1a** (40 mM) with 1-octanethiol (400 mM, 10 eq) in ACN under a 365 nm-centered LED, with yields quantified by HPLC against an internal standard.

In individual experiments, alcohol afforded only trace amounts of O-H-insertion product (<2%), while the N-H-insertion product reached a maximum value of 5% with diazirine **1b**. Under similar conditions, thiol-based adducts **2a** and **2b** were produced with highest yields (20-22%). Competitive reactions confirmed this tendency with the formation of small amounts of amines **3a**-**b** and ethers **4a**-**b** (<2%), whereas thioethers **2a**-**b** were formed in 15-26% yield. From this study, it was also noticed that ~ 4 min were required for complete diazirine photolysis and to reach the plateau of thioether **2a** formation (Figure 3c).

Next, carbonic anhydrase (bCA-II) was selected as model enzyme to demonstrate this proof-of-concept. First, the impact of light irradiation on the biological activity of this enzyme was investigated, and no loss of activity was observed after 5 minutes of irradiation at 365 nm (Figure 4). Under more extreme conditions (20 minutes of irradiation), ~80% of activity was still preserved. This study shows that the activation window for diazirine excitation is sufficiently broad to ensure efficient carbene formation while minimizing the damages on the protein target.

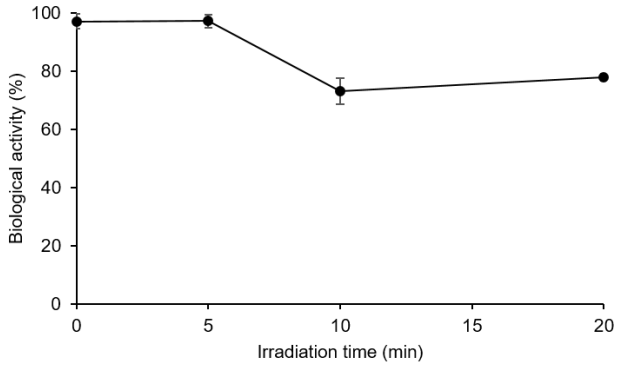

Figure 4. Monitoring residual biological activity as a function of irradiation time under a 365 nm-centered LED. Experiments were triplicated, and the results are presented as mean ± standard deviation (SD). *p*-Nitrophenyl acetate was used as the substrate for detecting the catalytic activity of bCA-II in Tris buffer (pH 7.5, 50 mM) by monitoring the increase in absorbance at 348 nm.

In situ photoassembly of an inhibitor of bCA-II

Then, a library of differently substituted aryl trifluoromethyl diazirines **1a**-**1f** (400 µM) was investigated in a one-to-one mixture with α-mercaptotosylamide **5** (60 µM), the latter serving as the anchor molecule (Figure 5a) through the complexation of the sulfonamide onto the catalytic Zn^{2+} atom. After 5 minutes of irradiation at room temperature, photo-KTGS mixtures were treated and analyzed by LC/MS in the single-ion monitoring mode (SIM). Out of the six possible ligands, one was unambiguously templated by bCA-II. The formation of compound **2d** was significantly accelerated in the presence of bCA-II compared to standard control experiments carried out either in the absence of enzyme ('blank') or in the presence of both enzyme (30 µM) and a commercial inhibitor ethoxzolamide ('ETOX', 200 µM) (Figures 5b-c). The representative LC/MS–SIM of the photo-KTGS carried out with the diazirine **2d** (*m/z* 403.9 ± 2, $[M-H]^-$) also exhibits a large peak corresponding to the **5**-**5** disulfide (*m/z* 403.0, $[M-H]^-$), a by-product observed along with the hydrated carbene product and diazo isomer of **2d** (see Figure S50a). A kinetic study reveals that the formation of the product **2d** reaches a plateau (300-400 nM, corresponding to 1% of the enzyme used) within a minute at room temperature and within a few minutes under controlled conditions (temperature set at 20 °C) (see figures S51-54).

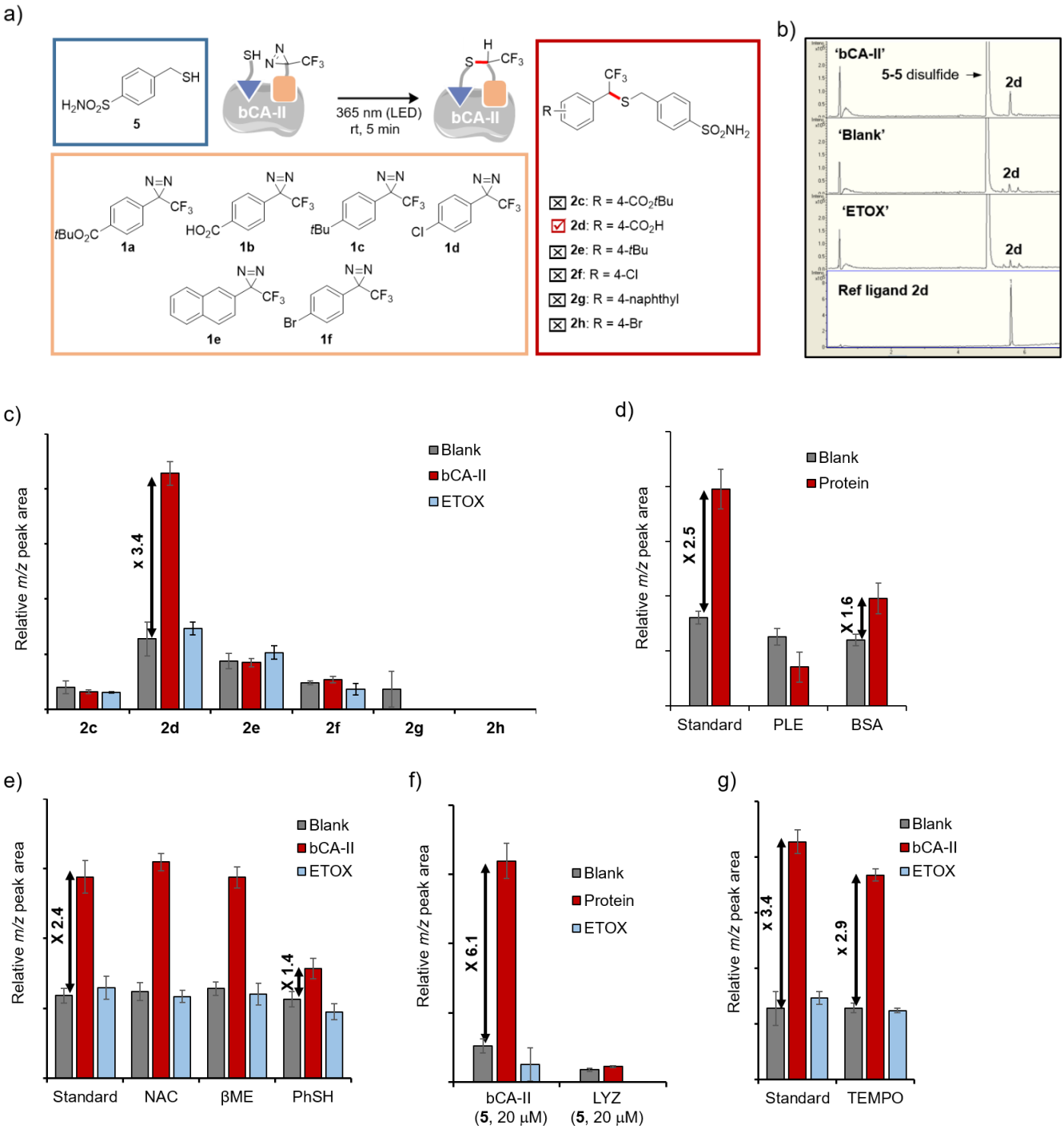

Figure 5. a) Library of photo-KTGS experiments between diazirines **1a**-**1f** (400 μM), thiol **5** (60 μM), carried out w bCA-II ('bCA-II',30 μM) or w/o ('blank'), or w bCA-II (30 μM) and ethoxzolamide ('ETOX', 200 μM) at rt upon light irradiation (365 nm-centered LED) (='standard'). Representative example of LC/MS in the single-ion (SIM *m/z* 403.9 ± 2 $[M-H]^-$) mode of photo-KTGS for ligand **2d**. Histograms obtained from LC/MS-SIM analyses showing the relative abundance of: c) each product **2c**-**2h** obtained under aforementioned conditions ('standard'); d) product **2d** obtained under aforementioned conditions ('standard') or in the presence of porcine liver esterase ('PLE', 30 μM) or bovine serum albumin ('BSA', 30 μM) instead of bCA-II (30 μM); e) product **2d** obtained under aforementioned conditions ('standard') or with the additional presence of competing thiols N-acetylcysteine ('NAC', 60 μM), or β-mercaptoethanol ('βME', 60 μM), or thiophenol ('PhSH', 60 μM); f) product **2d** obtained under aforementioned conditions ('standard') except thiol concentration set at 20 μM (instead of 60 μM); g) product **2d** obtained under aforementioned conditions ('standard') or with the additional presence of 2,2,6,6-tetramethylpiperidinyl-N-oxyl ('TEMPO', 800 μM) in 'blank', 'bCA-II' and 'ETOX'. All aforementioned experiments were triplicated, and the results are presented as mean ± standard deviation (SD).

A series of additional controls were conducted to further validate the successful ligation within the protein's active site and to gain insight into the scope and limitations of this photo-KTGS. First, no product **2d** was formed in the darkness or under laboratory ambient light. The KTGS carried out with sulfonamide-free benzyl mercaptan instead of α-mercaptotosylamide **5** did not yield more product in the presence of bCA-II (see Figure S41). Thus, the presence of the sulfonamide, which coordinates with the zinc active-site atom, is a prerequisite for bCA-II-mediated photoassembling. Note that the term 'standard' in Figures 5d-e and g refers to the successful ligation between diazirine **1b** and thiol **5** (Figure 5c), which was repeated along with other reactions conducted in the corresponding histograms. This aims to verify repeatability and compensate for minor variations that may occur over time among different assays. Photo-KTGS carried out in the presence of non-target proteins porcine liver esterase (PLE) and bovine serum albumin (BSA) confirmed that bCA-II was required to form product **2d** in higher amount(Figure 5d).

We thought that the addition of equimolar non-competing thiols (60 μM), without the sulfonamide group, would specifically decrease the background formation of product **2d** in control experiments 'blank' and 'ETOX'. This should, in turn, increase the ratio of **2d** between 'bCA-II' and the two controls. However, the presence of water-soluble N-acetylcysteine (NAC) or β-mercaptoethanol (βME) (60 μM) did not interfere either in the experiment carried out in the presence of the enzyme or in control experiments (Figure 5e). On the other hand, thiophenol noticeably reduced the amount of product formation only in the presence of the enzyme (from × 2.4 to × 1.4). This unexpected result was ascribed to a plausible thiophenol coordination to the zinc ion of the enzyme, thus competing with thiol **5**. This hypothesis was strengthened by Kaiser's work, which demonstrate that nitro thiophenol derivatives are effective inhibitors of bCA.[18]

Alternatively, to minimize non-specific product formation in 'blank' experiment (Figure 5f), the concentration of thiol anchor **5** in the medium, initially set at 60 μM (2 eq. relative to bCA-II), was reduced by threefold. Under these conditions, most of the thiol **5** should be bound to the active site of bCA-II. Satisfyingly, the ratio of product **2d** obtained in 'blank' versus in 'bCA-II' experiment improved from about 3 to 6, albeit with a lower signal-to-noise ratio (Figure S45). Furthermore, the reaction carried out in the presence of another readily available off-target, lysozyme ('LYZ'), instead of bCA-II, also failed to accelerate the product **2d** formation. As expected, the reaction with sulfonamide-free benzyl mercaptan under these diluted conditions did not yield more product in the presence of bCA-II than in the control experiments (see Figure S46).

Upon photoexcitation, diazirines are converted into ground state singlet carbenes, which are known to react efficiently with heteronucleophiles (X-H insertion) and undergo C-H insertion through a concerted mechanism. Such carbenes are characterized by short lifetime (~ ns time-scale) due to their rapid quenching in solution with adjacent water molecules, resulting in the formation of corresponding hydrated products. However, singlet carbenes can undergo spin equilibration to triplet carbenes, depending on the relative difference in their energy levels. Lifetime of triplet carbenes is much longer (~ μs time-scale), and react in a sequential hydrogen abstraction–radical recombination mechanism, which can lead to undesirable side reactions such as carbene homocoupling, carbene hydrogenation, and ketone formation from reaction of the carbene with molecular oxygen. To investigate whether the formation of the ligand **2d** predominantly proceeded through a singlet or triplet carbene intermediate, the KTGS was conducted using a radical scavenger known to interfere with triplet carbenes.[19] The presence of 2,2,6,6-tetramethylpiperidinyl-N-oxyl 'TEMPO' (800 μM, 2 eq. relative to diazirine) did not significantly alter the successful outcome of KTGS with diazirine **1b**, indicating that singlet carbene is presumably the predominant reactive species leading to the formation of product **2d** (Figure 5g).[20] Additionally, we also observed a significant formation of the hydrated carbene product in KTGS experiments (see Figure S50), in accordance with the singlet carbene mechanism. Nevertheless, the occurrence of an oxygen triplet cannot be ruled out, as the corresponding ketone was also detected, albeit in trace amounts (see Figure S50).

The presence of the trifluoromethyl group on the diazirine moieties could be leveraged to further confirm specific interactions between the bCA-II's active site and diazirine **1b**. ^{19}F NMR spectroscopy has emerged as a powerful tool for fragment screening in FBDD.[21] Although it has sensitivity comparable to that of ^{1}H, fluorine offers a broader spectral range (20 times wider), and the absence of fluorine atoms in proteins and buffers helps preventing signal overlap issues. We then decided to use a method based on monitoring ^{19}F NMR chemical shift and relaxation time T_2 (^{19}F) to confirm the presence or absence of an interaction between the bCA-II and diazirine **1b**. To achieve this, 1D ^{19}F and FAXS NMR experiments[22] were conducted on **S1-S3** solutions in PB buffer [**1b** (400uM) (**S1**), **1b** (400uM) in the presence of bCA-II (30uM) (**S2**), **1b** (800uM) in the presence of bCA-II (30uM) (**S3**)] . The 1D ^{19}F NMR spectra of the **S2** and **S3** mixtures compared to the **S1** spectrum shows fluorine chemical shift variations and the absence of new signals characteristic of **1b**/bCA-II complex formation (Figure 6). Observing only one signal for the free and bound **1b** species, that shifts depending on the **1b**:bCA-II molar ratio, shows that the binding equilibrium is fast on the ^{19}F NMR chemical shift time scale. These findings were further supported by measuring the relaxation time T_2 (^{19}F) of free diazirine **1b** (**S1**, T_2=1.68 s) and in the presence of bCA-II (**S2**, T_2=1.05 s) (Figure S57). As anticipated, a decrease in the relaxation time T_2 (^{19}F) was observed in the presence of bCA-II, indicating an interaction between bCA-II and diazirine **1b** resulting in a shorter T_2 transfer from bCA-II to the diazirine **1b** moieties.

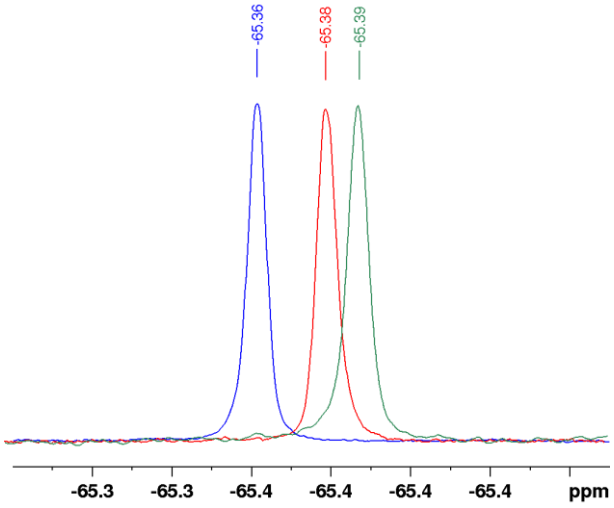

Figure 6. 1D ^{19}F spectra recorded at 476 MHz and 298K of a CF_3 containing **1b** molecule in the absence (S1, green), and presence (S2, red and S3, blue) of the bCA-II protein. The concentrations of **1b** in S1, S2 and S3 solutions were 400 μM, 400 μM and 800 μM, respectively. The concentration of bCA-II in S2 and S3 was 30 μM.

In order to gain a better understanding of the interaction between diazirine **1b** and bCA-II, and to pinpoint the exact site of interaction, a similar analytical approach was utilized. This involved the use of 1D ^{19}F and FAXS NMR spectroscopy to investigate the potential competition between diazirines **1b** and **1c (S4-S6**), as well as ethoxzolamide (**S3, S7**), in their interactions with bCA-II [[**1c** (400uM) (**S4**), **1c** (400uM) in the presence of bCA-II (30uM) (**S5**), **1b** (400uM), **1c** (400uM) in the presence of bCA-II (30uM) (**S6**) and **1b** (400uM), ethoxzolamide (400uM) in the presence of bCA-II (30uM) (**S7**)]. Our findings suggest that diazirine **1c** exhibits an interaction with bCA-II, as evidenced by chemical shift changes and significant broadening of the fluorine signal of **1c** (Figure S58). Interestingly, it was also observed that the interaction site of **1c** with bCA-II differs from that of diazirine **1b**, as demonstrated by the lack of any impact on the relaxation time of the fluorine signal of diazirine **1b** bound to bCA-II (T_2=1.08 s) when in presence of **1c** (Table 1). On the other hand, the addition of ethoxzolamide to **S2** solution results in an increase in the fluorine relaxation time of diazirine **1b**, T_2=1.43 s (**S7**), instead of 1.05 s (**S3**) (Table 1), suggesting a competitive binding scenario between diazirine **1b** and ethoxzolamide for interaction with bCA-II, with ethoxzolamide outcompeting diazirine **1b** at the binding site. In conclusion of this part, this study confirms the specific interactions between **1b** and the bCA-II active site.

Table 1. Fluorine relaxation times T_2 of a CF_3 containing **1b** molecule in the absence (S1) and presence (S3) of the bCA-II protein, in the presence of bCA-II protein and **1c** (S6) and in the presence of bCA-II protein and ethoxzolamide ligand (S7).

	S1	S3	S6	S7
T_2 (s)	1.68 s	1.05 s	1.08 s	1.43 s

Enantioselective synthesis of both enantiomers of ligand 2d for the determination of enantiomeric excess & biological activity

The Photo-KTGS we implemented leads to the formation of a stereogenic center through carbene insertion into S-H bond. Therefore, it is crucial to be able to provide synthetic access to each enantiomer of templated ligands. It will enable the determination of their respective biological activities and ascertain whether photo-KTGS favours the formation of one enantiomer, and if so, which one. Asymmetric carbene X-H insertion reactions with high enantiocontrol are challenging to achieve due to the inherent high reactivity of carbene species.[23] In order to obtain pure enantiomers, we decided to develop a stereodivergent synthesis based on the enantioselective reduction of a readily available common ketone intermediate **6** (Scheme 1).

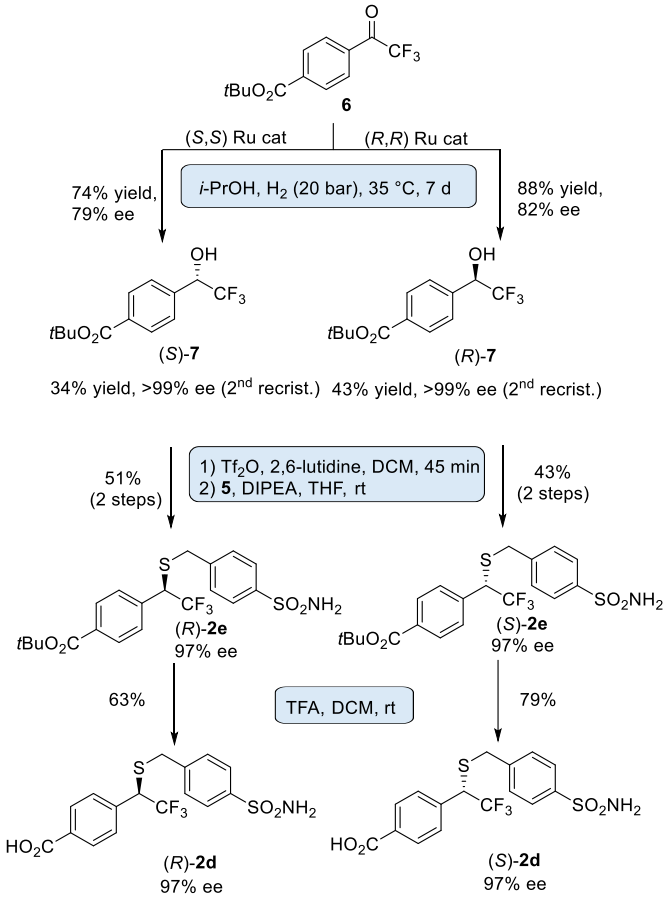

Scheme 1. Synthetic route for the preparation of both enantiomers (*R*)-**2d** and (*S*)-**2d** of **2d**.

This was achieved by using the Noyori asymmetric hydrogenation reaction, leveraging its practical applicability (scalability, low catalyst loading), generally high enantioselectivity, and the commercial availability of both enantiomers of the Ru complex catalyst.[24] Hydrogenation of the 2,2,2-trifluoroacetophenone **6** in the presence of Ru(Cl_2)[(*R*)-BINAP][(*R*)-Daipen] ((*R*,*R*) Ru cat) led to the corresponding alcohol (*R*)-**7** in 88% yield and 82% ee. Double recrystallization from heptane afforded the (trifluoromethyl)benzyl alcohol (*R*)-**7** in

43% overall yield with >99 ee. The absolute configuration was confirmed by determining the specific rotation of the corresponding deprotected carboxylic acid compound and comparing to published data.[25] After activation of the hydroxyl group to afford (*R*)-**2e**, the corresponding triflate was displaced with α-mercaptotosylamide **5** in THF in the presence of DIPEA to produce the corresponding thioether (*S*)-**2d** with 97% ee after carboxylic acid deprotection under acidic conditions. The ee value of triflate (S)-**2e** could not be determined due to instability issues during the HPLC separation of enantiomers. However, the slight erosion of the ee value (from >99 to 97%) may more likely result from the thiol-mediated S_N2 reaction.[26] Then, the same protocol was used to form the enantiomeric ligand (*R*)-**2d** starting from (S,*S*) Ru cat, $Ru(Cl_2)$[(*S*)-BINAP][(*S*)-Daipen] which was obtained with the same optical purity.

With both enantiomers (*S*)- and (*R*)-**2d** as authentic standards in hand, photo-KTGS reactions between **1b** and **5** carried out under standard conditions (Figure 5), were subsequently analyzed using a chiral LC-MS/MS method (Figure 7). The MS/MS experiment, targeting the specific transition *m/z* 403.9 $[M-H]^-$ –> 360.0 $[M-H-CO_2]^-$, was necessary to eliminate the **5**-**5** disulfide by-product, which overlapped with ligands **2d**, when using the chiral RP-HPLC column (see Figures S59-61). First, as expected, more ligand was formed in the presence of the enzyme than in controls, and both enantiomers are templated by bCA-II. According to the reference compounds, the first and second peak were unambiguously assigned to the (*R*)-**2d** and (*S*)-**2d** enantiomer, respectively. Importantly, while in controls ee values are close to zero, about 10% ee in favour of the (*R*)-**2d** enantiomer was observed in the presence of bCA-II (data given as mean value from triplicate experiments, Table 2). This result suggests that the chiral environment of the active site may be the source of selectivity, albeit very modest. In fact, a direct comparison with control experiments shows that both enantiomers were significantly templated by bCA-II.

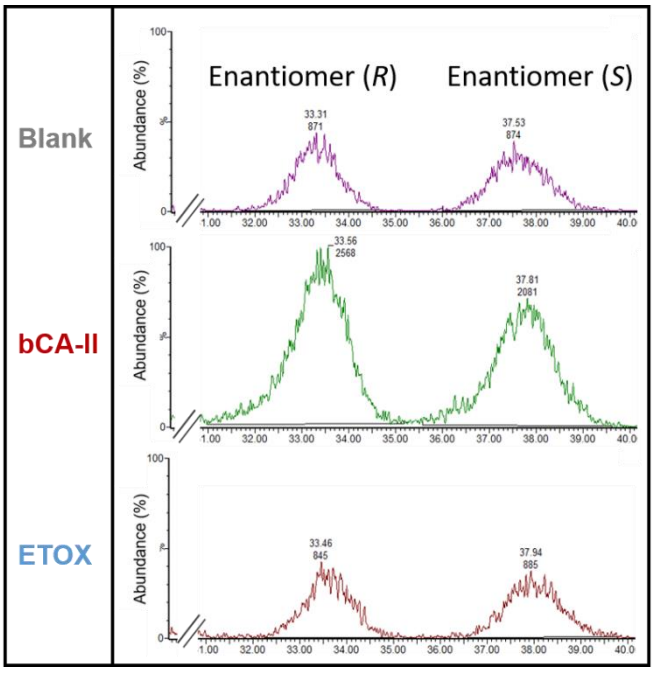

Figure 7. Representative example of LC/MS-MS chromatograms of **2d** (specific transition: m/z 403.9 $[M-H]^-$ –> 360.0 $[M-H-CO_2]^-$) obtained from photo-KTGS experiments carried out between **5** and **1b**. These reactions were run and analyzed in triplicate.

Table 2. Relative abundance of enantiomers (*R*)-**2d** and (*S*)-**2d** obtained through photo-KTGS between **1b** and **5**.[a]

	Enantiomer (*R*) (%)	Enantiomer (*S*) (%)	Ee (%)[b]
Blank	48.2±0.6	51.8±0.6	3.6±1.2 (S)
bCA-II	55.4±0.7	44.6±0.7	10.8±1.5 (R)
ETOX	49.9±0.4	50.1±0.4	0.8±0.4 (S)

[a] All reactions were run and analyzed in triplicate. [b] Determined by LC/MS-MS analysis equipped with a chiral stationary phase.

Next, the biological activity of sulfonamide ligands, whether photo-assembled in the presence of bCA-II (**2d**) or not (**2c**, **2e-f**, **2h**), was determined to evaluate the substituent effect on their inhibitory activity (Figure 8). The esterase activity was monitored by using the chromogenic substrate 4-nitrophenylacetate.[27]

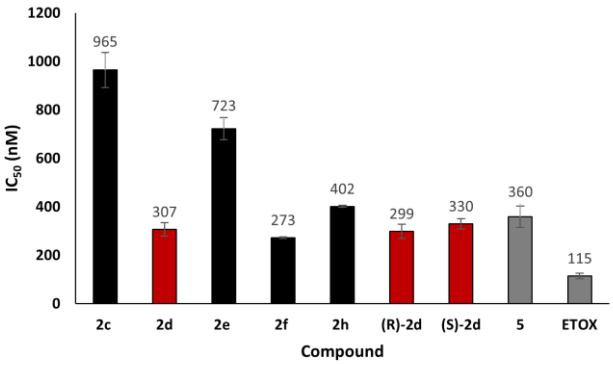

Figure 8. Histogram of the IC_{50} values of ligands (templated by bCA-II, in red, and not templated by bCA-II, in black), as well as those of the starting thiol **5** and the commercial inhibitor ETOX (in grey). *p*-Nitrophenyl acetate was used as the substrate for detecting the catalytic activity of bCA-II in Tris buffer (pH 7.5, 50 mM) by monitoring the increase in absorbance at 348 nm.

IC_{50} values of sulfonamide ligands are within the 273–965 nM range. For comparison, the clinical inhibitor ethoxzolamide **ETOX** has an IC_{50} value of 115±12 nM. Compound **2c** substituted at the position 4 by an electron-withdrawing *tert*butyl ester group exhibits the lowest activity with an IC_{50} value close to 1 μM. In contrast, the photo-assembled compound (±)-**2d**, which bears a carboxylic acid group, ranks among the most bioactive ligands (307 nM). Compound **2e**, substituted with an electron-donating *tert*-butyl group, exhibits the second lowest inhibitory activity in the series, with an IC_{50} value of 723 nM. The ligand **2h**, substituted with a bromide, exhibits weaker activity (402 nM) compared to the chloride compound **2f** (273 nM). Overall, these

results suggest that biological activity decreases as the size of the substituent increases, with the exception of the carboxylic acid substituent, which can establish hydrogen bond interactions with the protein. Additionally, the inhibitory activities of both enantiomers, (*R*)-**2d** and (*S*)-**2d**, were comparable and within the range of that exhibited by the anchor fragment **5**. The non-trifluoromethylated analog of **2d** (compound **S24**, Figure S62) exhibits an IC_{50} value of 239 nM. These latter results show that the presence of the trifluoromethyl group and its stereochemistry do not improve the biological activity, and could provide a plausible explanation for the low ee observed in favor of (*R*)-**2d** in photo-KTGS. Besides, no inhibitory activity was detected at 800 mM for the diazirine partner **1b**, although the ^{19}F NMR experiments proved that **1b** is able to bind to CAII. A plausible low binding might explain the modest yield enhancement for the templated formation of **2d**.

Conclusion

Herein, we report the identification of a sulfonamide-based inhibitor of bCA-II using a KTGS approach associated for the first time with photochemistry (photo-KTGS). This combination enabled a fast ligation reaction (within one minute) between *in situ* generated carbene and thiol partners, while minimizing product formation in controls. The success of this approach depends on both the rapid quenching of the carbene intermediate by water molecules outside the protein, as well as the rapid reaction of thiols with the carbene inside the protein. Photo-KTGS still generates more ligand molecule in the blank compared to what *in situ* click chemistry does, which might be due to the limited affinity of the aziridine moiety for the protein. However, working under more diluted conditions allowed us to mitigate non-specific ligand formation. Of note, the photo-KTGS reaction was not disrupted by the presence of thiols unable to bind the protein in the medium, enabling us to consider this reaction, in more complex environments. At terms, such a photo-KTGS strategy should also be combined to the highly promising and elegant approach of DNA-encoded dynamic libraries (DEDLs), as recently suggested their authors Li and colleagues.[28]

The ligation reaction between fragments results in the formation of a stereogenic center, whose absolute configuration can potentially be controlled by the protein target. Furthermore, such chirality could be exploited for the design of ligands better covering the three-dimensional chemical space of proteins than sp^2-based compounds.[29] Between 2015 – June 2020, 63% (103 out of 164) of FDA approved small-molecules were chiral. However, two enantiomers can exhibit different pharmacodynamics, pharmacokinetics, and toxicity.[30] To address this challenge, alongside the development of the photo-KTGS methodology, an enantioselective approach has been established for both enantiomers of the *in situ* formed ligand.

The presence of the trifluoromethyl group is crucial for stabilizing the carbene intermediate, preventing intramolecular reactions, and rendering the diazo isomer inert. Furthermore, the trifluoromethyl group could be advantageously used to fine-tune the chemical library of TPD-based fragments capable of interacting with the POI active site, as demonstrated through a ^{19}F NMR binding assay. Moreover, it can contribute as a benefit to the final ligand structure, providing favorable interactions with the POI, influencing physicochemical properties, and improving adsorption, distribution, metabolism, and excretion (ADME) characteristics.[31]

Over the last 30 years, numerous TPD-based probes or ligands have been developed for photoaffinity labelling studies. These derivatives could be repurposed as anchor molecules in future photo-KTGS experiments, enabling the discovery of ligands with enhanced biological properties or the development of multi-target directed ligands.

Supporting Information

All the data that support these studies such as experimental protocols, NMR spectra, HPLC traces, MS data are available in the supplementary material of this article. The authors have cited additional references within the Supporting Information.[32-35]

Acknowledgements

This work has been partially supported by University of Rouen Normandy, INSA Rouen Normandy, the Centre National de la Recherche Scientifique (CNRS), European Regional Development Fund (ERDF), Labex SynOrg (ANR-11-LABX-0029), Carnot Institute I2C, the graduate school for research XL–Chem (ANR-18-EURE-0020XL CHEM), by Normandy Region. We are grateful to Emilie Petit (INSA de Rouen) and Albert Marcual (CNRS) for HPLC and high-resolution mass spectrometry analyses, respectively. We also thank Françoise Ringot (URN) for the determination of physicochemical properties.

Keywords: kinetic target-guided synthesis • photo-assembly • photochemistry • diazirine • carbonic anhydrase

[1] D. A. Erlanson, S. W. Fesik, R. E. Hubbard, W. Jahnke, H. Jhoti, *Nat. Rev. Drug. Discov*. **2016**, *15*, 605-619.

[2] E. V. Bedwell, W. J. McCarthy, A. G. Coyne, C. Abell, *Chem. Biol. Drug Des.* **2022**, *100*, 469-486.

[3] O. Ichihara, J. Barker, R. J. Law, M. Whittaker, *Mol. Inform*. **2011**, *30*, 298-306.

[4] a) D. Bosc, V. Camberlein, R. Gealageas, O. Castillo-Aguilera, B. Deprez, R. Deprez-Poulain, *J. Med. Chem*. **2020**, *63*, 3817-3833; b) P. T. Parvatkar, A. Wagner, R. Manetsch, *Trends Chem*. **2023**, *5*, 657-671.

[5] E. Oueis, G. Santoni, C. Ronco, O. Syzgantseva, V. Tognetti, L. Joubert, A. Romieu, M. Weik, L. Jean, C. Sabot, F. Nachon, P. Y. Renard, *Org. Biomol. Chem*. **2014**, *12*, 156-161.

[6] W. G. Lewis, L. G. Green, F. Grynszpan, Z. Radić, P. R. Carlier, P. Taylor, M. G. Finn, K. B. Sharpless, *Angew. Chem. Int. Ed.* **2002**, *41*, 1053-1057.

[7] a) Y. Bourne, H. C. Kolb, Z. Radic, K. B. Sharpless, P. Taylor, P. Marchot, *Proc. Natl. Acad. Sci. U S A* **2004**, *101*, 1449-1454; b) C. Ronco, E. Carletti, J. P. Colletier, M. Weik, F. Nachon, L. Jean, P. Y. Renard, *ChemMedChem* **2012**, *7*, 400-405; c) Y. Bourne, K. B. Sharpless, P. Taylor, P. Marchot, *J. Am. Chem. Soc*. **2016**, *138*, 1611-1621.

[8] K. B. Sharpless, R. Manetsch, *Expert Opin. Drug Discov*. **2006**, *1*, 525-538.

[9] R. Nguyen, I. Huc, *Angew. Chem. Int. Ed.* **2001**, *40*, 1774-1776.

[10] E. Oueis, F. Nachon, C. Sabot, P. Y. Renard, *Chem Commun (Camb)* **2014**, *50*, 2043-2045.

[11] X. Hu, J. Sun, H. G. Wang, R. Manetsch, *J. Am. Chem. Soc.* **2008**, *130*, 13820-13821.

[12] A. Lossouarn, P. Y. Renard, C. Sabot, *Bioconjugate Chem*. **2021**, *32*, 63-72.

[13] J. Brunner, H. Senn, F. M. Richards, *J. Biol. Chem*. **1980**, *255*, 3313-3318.

[14] C. Iacobucci, M. Gotze, C. Piotrowski, C. Arlt, A. Rehkamp, C. Ihling, C. Hage, A. Sinz, *Anal. Chem*. **2018**, *90*, 2805-2809.

[15] A. Admasu, A. D. Gudmundsdóttir, M. S. Platz, D. S. Watt, S. Kwiatkowski, P. J. Crocker, *J. Chem. Soc., Perkin Trans. 2*, **1998**, 1093-1100.

[16] T. Suzuki, T. Okamura, T. Tomohiro, Y. Iwabuchi, N. Kanoh, *Bioconjugate Chem*. **2015**, *26*, 389-395.

[17] A. V. West, G. Muncipinto, H. Y. Wu, A. C. Huang, M. T. Labenski, L. H. Jones, C. M. Woo, *J. Am. Chem. Soc*. **2021**, *143*, 6691-6700.

[18] J. Olander, E. T. Kaiser, *Biochem. Biophys. Res. Commun*. **1971**, *45*, 1083-1088.

[19] J. Nakajima, K. Hirai, H. Tomioka, *Org. Biomol. Chem.* **2004**, *2*, 1500-1503.

[20] J.-i. Nakajima, K. Hirai, H. Tomioka, *Org. Biomol. Chem.* **2004**, *2*, 1500-1503.

[21] C. R. Buchholz, W. C. K. Pomerantz, *RSC Chem. Biol*. **2021**, *2*, 1312-1330.

[22] C. Dalvit, M. Flocco, M. Veronesi, B. J. Stockman, *Comb. Chem. High Throughput Screen*. **2002**, *5*, 605-611.

[23] W. Guo, Y. Zhou, H. Xie, X. Yue, F. Jiang, H. Huang, Z. Han, J. Sun, *Chem. Sci*. **2023**, *14*, 843-848.

[24] T. Ohkuma, M. Koizumi, H. Doucet, T. Pham, M. Kozawa, K. Murata, E. Katayama, T. Yokozawa, T. Ikariya, R. Noyori, *J. Am. Chem. Soc*. **1998**, *120*, 13529-13530.

[25] A. S. Rowan, T. S. Moody, R. M. Howard, T. J. Underwood, I. R. Miskelly, Y. A. He, B. Wang, *Tetrahedron: Asymmetry 2013*, **24**, 1369-1381.

[26] G. Hughes, P. O'Shea, J. Goll, D. Gauvreau, J. Steele, *Tetrahedron* **2009**, *65*, 3189-3196.

[27] A. Lossouarn, C. Puteaux, L. Bailly, V. Tognetti, L. Joubert, P. Y. Renard, C. Sabot, *Chem. Eur. J.* **2022**, *28*, e202202180.

[28] Y. Zhou, W. Shen, Y. Gao, J. Peng, Q. Li, X. Wei, S. Liu, F. S. Lam, J. Mayol-Llinas, G. Zhao, G. Li, Y. Li, H. Sun, Y. Cao, X. Li, *Nat. Chem*. **2024**, *16*, 543–555.

[29] B. Over, S. Wetzel, C. Grutter, Y. Nakai, S. Renner, D. Rauh, H. Waldmann, *Nat. Chem*. **2013**, *5*, 21-28.

[30] P. Bhutani, G. Joshi, N. Raja, N. Bachhav, P. K. Rajanna, H. Bhutani, A. T. Paul, R. Kumar, *J. Med. Chem.* **2021**, *64*, 2339-2381.

[31] a) E. Berrino, B. Michelet, A. Martin-Mingot, F. Carta, C. T. Supuran, S. Thibaudeau, *Angew. Chem. Int. Ed*. **2021**, *60*, 23068-23082; b) A. S. Nair, A. K. Singh, A. Kumar, S. Kumar, S. Sukumaran, V. P. Koyiparambath, L. K. Pappachen, T. M. Rangarajan, H. Kim, B. Mathew, *Processes* **2022**, *10*, 2054.

[32] K. Sakurai, T. Yasui, S. Mizuno, *Asian J . Org. Chem*. **2015**, *4,* 724-728.

[33] S. F. Musolino, Z. Pei, L. Bi, G. A. DiLabio, J. E. Wulff, *Chem. Sci*. **2021**, *12*, 12138-12148.

[34] R. Stewart, K. C. Teo, *Can. J. Chem*. **1980**, *58*, 2491-2496.

[35] Y. Pocker, J. T. Stone, *Biochemistry* **1967**, *6*, 668-678.

Light-Induced Unlocking Reactivity of Fragments for Fast Target-Guided Synthesis of Carbonic Anhydrase Inhibitors.

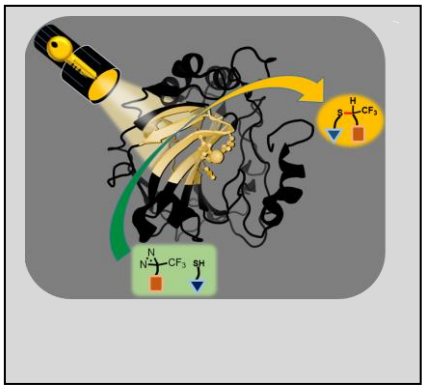

By integrating photochemistry within kinetic target-guided synthesis (KTGS) techniques, we significantly accelerated the identification of enzyme inhibitors, demonstrating the potential of KTGS for rapid discovery of bioactive ligands in medicinal chemistry. The chiral linkage gives rise to the formation of enantiomers, which were assessed *via* a highly stereocontrolled synthesis of both templated ligand enantiomers.